European Journal of Mechanics B/Fluids 38 (2013) 114–127

Contents lists available at SciVerse ScienceDirect

European Journal of Mechanics B/Fluids

journal homepage: www.elsevier.com/locate/ejmflu

Rarefied gas flow through a cylindrical tube due to a small pressure difference

Sarantis Pantazis *, Dimitris Valougeorgis

University of Thessaly, Department of Mechanical Engineering, Volos 38334, Greece

ARTICLE INFO

Article history:
Received 3 June 2012
Received in revised form
4 October 2012
Accepted 26 October 2012
Available online 16 November 2012

Keywords:
Linearized flow
Kinetic theory
Microflows
Vacuum flows
Knudsen number

ABSTRACT

Flow of a rarefied gas through a cylindrical tube connecting two reservoirs maintained at a small pressure difference is considered using the axisymmetric version of the linearised BGK kinetic model equation subject to Maxwell diffuse–specular boundary conditions. This is a problem of five dimensions in phase space, solved in a fully deterministic manner using a parallelised discrete velocity algorithm. Results include flow rates as well as distributions of density and velocity perturbations, from the free molecular up to the slip regime and for length-over-radius (L/R) ratios ranging from zero (orifice flow) up to 20. The dependency of the results on gas rarefaction, wall accommodation and tube length is analysed and discussed. It is found that the Knudsen minimum appears only at $L/R = 20$. Furthermore, in the case of $L/R = 0$ it is confirmed that the results are practically independent of the accommodation coefficient. Comparing the present linear results with corresponding non-linear ones, it is seen that linearised analysis can capture the correct behaviour of the flow field not only for infinitesimally small but also for small but finite pressure differences and that its range of applicability is wider than expected. Also, the error introduced by the assumption of fully developed flow for channels of moderate length is estimated through a comparison with the present corresponding results.

1. Introduction

The flow of a rarefied gas through long or short cylindrical tubes (including orifices) due to small or large pressure differences is of major importance in the design and optimisation of various types of industrial equipment in several technological fields. Some of these applications include mass flow controllers in gas metering [1], mass spectrometric sampling [2], micropropulsion in high altitude and space gas dynamics [3], pumps and gas distribution in vacuum systems [4–6], membranes and porous media in filtering [7,8], gaseous devices in microelectromechanical systems [9,10] and others [11–13]. Rarefied gas flows through tubes also have a strong theoretical interest, mainly due to the fact that a relatively small number of geometric and flow parameters is adequate to fully define the problem. The study of such flows has allowed the investigation of many non-equilibrium phenomena in the whole range of the Knudsen number. In addition, they have been applied as prototype problems to test the validity of proposed kinetic equations, gas-surface scattering kernels and intermolecular collision models, as well as to benchmark the computational efficiency of various numerical schemes.

Fully developed flows in long channels, i.e. in channels where the ratio of the length over the hydraulic diameter is large (a safe estimate is about 100 or more), have been considered by many researchers [14–16] and for various geometries [17–22], both numerically and experimentally. This flow configuration may be considered as the simplest one, since channel end effects are neglected and the pressure varies only in the flow direction. The kinetic solution is obtained only on a cross section of the channel for a wide range of the Knudsen number and then the solution for the whole flow field is obtained via a well-known methodology based on mass conservation [15,23]. Both for small and large pressure drops between the inlet and outlet pressure, the local pressure gradient is small and linearised kinetic analysis may be applied in a computationally efficient manner, yielding very accurate results. Experimental work in flows through long channels has also been performed and very good agreement between measurements and computations has been obtained [22,24–26].

The corresponding flow through short channels poses much larger computational difficulties due to the increased dimensionality of the problem and more importantly due to the fact that end effects must be considered in the simulation by including adequately large parts of the upstream and downstream containers in the computational domain. As a result, the required simulation time is significantly increased. Early works investigate slit and orifice flows near the free molecular regime [27–29], with particular emphasis on flow into vacuum, but their range of applicability is small. In order to obtain the behaviour of the flow for any rarefaction regime, the most commonly implemented and successful approaches rely on the Direct Simulation Monte Carlo (DSMC) method [30]. At large pressure differences, DSMC has been used, due to its simplicity and high accuracy, in the whole range of rarefaction for the

* Correspondence to: Physikalisch-Technische Bundesanstalt, Berlin 10587, Germany. Tel.: +49 3034817210.
E-mail address: sarantis.pantazis@ptb.de (S. Pantazis).

0997-7546/$ – see front matter © 2012 Elsevier Masson SAS. All rights reserved.
doi:10.1016/j.euromechflu.2012.10.006

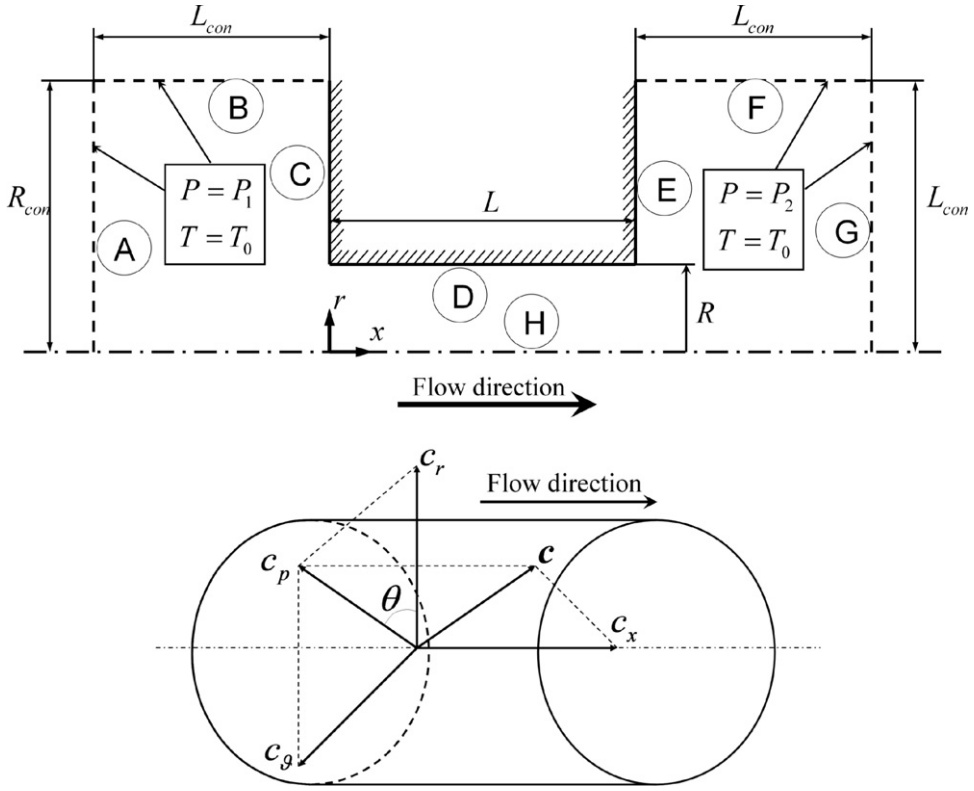

Fig. 1. Geometry and coordinate systems.

solution of high speed flows through slits [31–33], orifices [3,34,35] and short channels [33,36,37]. These works have limitations in the small pressure difference range and the investigations closest to the present work were conducted by Sharipov [35] for orifice flow with values of pressure ratio up to 0.9. It is well known that DSMC, at least in its original version, is not suitable for the simulation of low speed flows. Non-linear kinetic model equations tackled by the Discrete Velocity Method (DVM) have also been applied in [38–43] for problems of plane and axisymmetric geometry (slits, plates, orifices and tubes) and this approach could alternatively be used for any value of pressure ratio.

In the case of small pressure differences, the literature is rather limited. Akin'shin et al. [44] have solved the linearised non-isothermal slit problem by the integral moment method employing the Shakhov kinetic model [45,46]. Flow through a slit has also been examined by Hasegawa and Sone [47] for small pressure differences with the BGK model. Sharipov has applied the DVM to solve the linearised isothermal [48] and non-isothermal [49] slit problem, where the satisfaction of the Onsager theorem is verified. Shakhov solved the problem of linearised isothermal flow in channels [50,51] and also compared with the fully developed flow in a slightly different manner [50]. This procedure significantly reduced the difference between the two approaches but a prior knowledge of the pressure gradient is required, which is difficult to obtain without the complete numerical simulation.

There are several experimental investigations regarding flow through slits and orifices [1,52]. Results include mass flow rates, discharge coefficients and interpolating formulas. Tubes of small length-to-radius ratios have also been studied experimentally by Sreekanth [53], Fujimoto and Usami [54], Marino [55] and Varoutis et al. [56] for a wide range of pressure ratios in the transition regime. However, very few works deal with low pressure differences [57,58].

In this work, we apply a parallelised DVM algorithm to investigate flows through circular tubes driven by small pressure differences in a wide range of the Knudsen number. The tube geometry ranges from orifice up to a length-over-radius ratio equal to 20 and the channel end effects are considered by including a part of the upstream and downstream containers. Low pressure differences have not been examined extensively in the past and a detailed study of this problem is important in order to obtain reliable solutions for conditions where the computational cost of DSMC is very high. Results are provided in dimensionless form for the flow rates and the macroscopic distributions and their dependency on gas rarefaction, wall accommodation and tube length is analysed and discussed. The range of applicability of linearised theory is examined via a comparison with non-linear BGK results. Also, the error introduced by the assumption of fully developed flow for channels of moderate length is estimated through a comparison with the corresponding present results.

2. Formulation

2.1. Flow configuration

Consider two reservoirs filled with a monatomic, rarefied gas at slightly different pressures and connected by a cylindrical tube through which flow is induced. The pressure of the upstream and downstream reservoirs is $P_1 = P_0 + \Delta P$ and $P_2 = P_0$ respectively, as seen in Fig. 1. The fields of all bulk quantities change only along the radial and axial directions, $\hat{r}$ and $\hat{x}$, while remaining constant in the azimuthal angle ϑ due to the axisymmetry. Therefore, in order to describe the geometry, only the tube length L and radius R are required. Even though all walls and reservoirs are maintained at a constant temperature T_0, small variations of temperature are expected in the flow field. Due to the relatively small length of the tube, the flow is not fully developed and therefore a portion of the two containers is included in the simulations in order to properly impose the boundary conditions and take into account the channel end effects.

The basic flow parameter is the reference rarefaction parameter δ, defined here as

$$\delta = \frac{RP_0}{\mu_0 \upsilon_0} \tag{1}$$

where μ_0 is the gas viscosity at reference temperature T_0 and $\upsilon_0 = \sqrt{2R_g T_0}$ is the most probable molecular velocity with R_g being the gas constant. It is noted that δ is inversely proportional to the Knudsen number.

The flow configuration is defined by the geometrical ratio L/R and the reference rarefaction parameter δ and the objective is to obtain the solution of this flow in terms of these two parameters.

2.2. Governing kinetic equations

For sufficiently long times and due to the nearly isothermal nature of the pressure driven flow, the steady state BGK kinetic model equation may be used

$$\xi_r \frac{\partial f}{\partial \hat{r}} - \frac{\xi_\vartheta}{\hat{r}} \frac{\partial f}{\partial \theta} + \xi_x \frac{\partial f}{\partial \hat{x}} = \nu \left(f^M - f\right) \tag{2}$$

where $\boldsymbol{\xi} = (\xi_r, \xi_\vartheta, \xi_x)$ is the molecular velocity vector and $\theta \in [0, 2\pi]$ is the corresponding angle in the $\hat{r} - \vartheta$ plane, f is the unknown distribution function and $\nu = P/\mu$ is the collision frequency. The Maxwellian distribution is defined by

$$f^M\left(\hat{x}, \hat{r}\right) = \frac{n\left(\hat{x}, \hat{r}\right)}{\left[2\pi R_g T\left(\hat{x}, \hat{r}\right)\right]^{3/2}} \exp\left\{-\frac{\left[\boldsymbol{\xi} - \hat{\boldsymbol{u}}\left(\hat{x}, \hat{r}\right)\right]^2}{2R_g T\left(\hat{x}, \hat{r}\right)}\right\}. \tag{3}$$

Macroscopic quantities, such as the number density $n\left(\hat{x}, \hat{r}\right)$, bulk velocity $\hat{\boldsymbol{u}}\left(\hat{x}, \hat{r}\right)$ and temperature $T\left(\hat{x}, \hat{r}\right)$, are obtained by taking appropriate moments of f. The coordinates in the physical $\left(\hat{x}, \hat{r}\right)$ and molecular velocity spaces $(\xi_r, \xi_\vartheta, \xi_x)$ are shown in Fig. 1 and constitute a five-dimensional phase space for the distribution function.

Since the pressure difference between the upstream and the downstream vessel is small ($\Delta P/P_0 \ll 1$), the distribution function can be linearised as

$$f = f_0\left(1 + h\Delta P/P_0\right) \tag{4}$$

with f_0 being a Maxwellian at the reference conditions.

All quantities are expressed in dimensionless form as follows:

$$\begin{aligned}
&r = \frac{\hat{r}}{R}, \qquad x = \frac{\hat{x}}{R}, \qquad \boldsymbol{c} = \frac{\boldsymbol{\xi}}{\upsilon_0}, \\
&\rho\left(x, r\right) = \frac{n\left(x, r\right) - n_0}{n_0} \frac{P_0}{\Delta P}, \\
&\tau\left(x, r\right) = \frac{T\left(x, r\right) - T_0}{T_0} \frac{P_0}{\Delta P}, \\
&p\left(x, r\right) = \frac{P\left(x, r\right) - P_0}{P_0} \frac{P_0}{\Delta P}, \qquad \boldsymbol{u}\left(x, r\right) = \frac{\hat{\boldsymbol{u}}\left(x, r\right)}{\upsilon_0} \frac{P_0}{\Delta P}
\end{aligned} \tag{5}$$

where $\rho, \tau, \boldsymbol{u}, p$ are the perturbations of density, temperature, velocity and pressure. The right container conditions are taken as reference quantities.

As a final step, the molecular velocity vector $\boldsymbol{c} = (c_r, c_\vartheta, c_x)$ is transformed to cylindrical coordinates $\boldsymbol{c} = \left(c_p, \theta, c_x\right)$. Thus, we obtain

$$\begin{aligned}
&c_p \cos\theta \frac{\partial h}{\partial r} - \frac{c_p \sin\theta}{r} \frac{\partial h}{\partial \theta} + c_x \frac{\partial h}{\partial x} + \delta h \\
&\quad = \delta\left[\rho + \tau\left(c^2 - \frac{3}{2}\right) + 2\boldsymbol{c} \cdot \boldsymbol{u}\right].
\end{aligned} \tag{6}$$

Similarly, the macroscopic quantity perturbations are expressed in terms of the perturbation h

$$\rho = \frac{1}{\pi^{3/2}} \int_{-\infty}^{\infty} \int_0^{2\pi} \int_0^{\infty} h c_p \exp\left(-c^2\right) dc_p d\theta dc_x \tag{7}$$

$$u_x = \frac{1}{\pi^{3/2}} \int_{-\infty}^{\infty} \int_0^{2\pi} \int_0^{\infty} h c_x c_p \exp\left(-c^2\right) dc_p d\theta dc_x \tag{8}$$

$$\begin{aligned}
u_r \;=\; &\frac{1}{\pi^{3/2}} \int_{-\infty}^{\infty} \int_0^{2\pi} \int_0^{\infty} h\left(c_p \cos\theta\right) c_p \\
&\times \exp\left(-c^2\right) dc_p d\theta dc_x
\end{aligned} \tag{9}$$

$$\begin{aligned}
\tau \;=\; &\frac{1}{\pi^{3/2}} \int_{-\infty}^{\infty} \int_0^{2\pi} \int_0^{\infty} h\left(\frac{2}{3}c^2 - 1\right) c_p \\
&\times \exp\left(-c^2\right) dc_p d\theta dc_x.
\end{aligned} \tag{10}$$

The perturbation of pressure is found by $p = \rho + \tau$. The macroscopic velocity vector has only two components $\boldsymbol{u} = (u_x, u_r)$ due to the axisymmetry of the flow. It is also noted that the pressure difference is not included in these expressions and is taken into account only during the dimensionalisation of results according to Eq. (5). This is typical in linear solutions.

The most important quantity for practical applications is the mass flow rate through the channel, defined by

$$\dot{M} = 2\pi m \int_0^R n\left(\hat{x}, \hat{r}\right) \hat{u}_x\left(\hat{x}, \hat{r}\right) \hat{r} d\hat{r} \tag{11}$$

with m being the molecular mass. The mass flow rate is linearised to yield

$$\dot{M}_{LIN} = 2\pi m n_0 \upsilon_0 \frac{\Delta P}{P_0} \int_0^1 u_x\left(x, r\right) r dr \tag{12}$$

and then the linearised mass flow rate is non-dimensionalised by the free molecular ($\delta = 0$) solution for flow through an orifice (a tube of zero length) given by $\dot{M}_{FM} = R^2 \sqrt{\pi} \Delta P/\upsilon_0$ [23], which can be easily extracted by the method of characteristics. Results are presented in dimensionless form according to

$$W_{LIN} = \frac{\dot{M}_{LIN}}{\dot{M}_{FM}} = 4\sqrt{\pi} G \tag{13}$$

where

$$G = \int_0^1 u_x\left(x, r\right) r dr \tag{14}$$

is the reduced flow rate. Even though the expression for G contains the axial velocity which depends on x, G (and W_{LIN}) is practically constant in any cross-section.

It is also noted that according to [48] the linearised analysis is valid when

$$\frac{\Delta P}{P_0} \ll 1 \tag{15}$$

for $\delta < 1$ and

$$\frac{\Delta P}{P_0} \delta^2 \ll 1 \tag{16}$$

for $\delta > 1$.

2.3. Boundary conditions

The formulation is completed by providing the boundary conditions. Molecules entering from the free surfaces (A), (B), (F), (G)

(as shown in Fig. 1) conform to a Maxwellian distribution according to the conditions of the corresponding vessel. Thus, for the left vessel, we have $n = n_0 + \Delta n$, $T = T_0$ and $\hat{\boldsymbol{u}} = 0$ and therefore the perturbation from the equilibrium distribution is

$$h^+_{A,B} = \rho_{in} = \frac{(n_0 + \Delta n) - n_0}{n_0\,(\Delta P/P_0)} = \frac{(P_0 + \Delta P) - P_0}{P_0\,(\Delta P/P_0)} = 1. \tag{17}$$

Similarly, it is found that in downstream free surfaces (F), (G) the perturbation of the incoming distribution is

$$h^+_{F,G} = 0. \tag{18}$$

For the walls (C), (D), (E), diffuse–specular boundary conditions are imposed, i.e.

$$h^+ = \alpha_M \rho_w + (1 - \alpha_M)\, h^- \tag{19}$$

where α_M is the Maxwell accommodation coefficient and h^- is the distribution of impinging particles. The ρ_w constants are found by imposing the impermeability condition ($u_n = 0$) and the velocity integrals (8)–(9). The final expression is

$$\rho_w = -\frac{I_{impinging} + (1 - \alpha_M)\, I_{specular}}{\alpha_M I_{departing}}. \tag{20}$$

The notation "impinging" refers to the distribution of molecules hitting the wall, while the words "specular" and "departing" denote the distribution of particles scattered specularly and non-specularly, respectively. The integrals of Eq. (20) are

$$I_{departing}\big|_a = \int_{c_{x1a}}^{c_{x2a}} \int_{\pi-\theta_{2a}}^{\pi-\theta_{1a}} \int_0^{\infty} \left[c_p \phi_a\left(\theta, c_p, c_x\right)\right] \times \exp\left(-c_p^2 - c_x^2\right) dc_p d\theta dc_x \tag{21}$$

$$I_{impinging}\big|_a = \int_{-c_{x2a}}^{-c_{x1a}} \int_{\theta_{1a}}^{\theta_{2a}} \int_0^{\infty} h^- \left[c_p \phi_a\left(\theta, c_p, c_x\right)\right] \times \exp\left(-c_p^2 - c_x^2\right) dc_p d\theta dc_x \tag{22}$$

$$I_{specular}\big|_a = \int_{c_{x1a}}^{c_{x2a}} \int_{\pi-\theta_{2a}}^{\pi-\theta_{1a}} \int_0^{\infty} h_{specular} \times \left[c_p \phi_a\left(\theta, c_p, c_x\right)\right] \exp\left(-c_p^2 - c_x^2\right) dc_p d\theta dc_x \tag{23}$$

where $a = C, D, E$ (see Fig. 1) and

$$\begin{aligned} &C: \theta_{1C} = 0, \quad \theta_{2C} = \pi, \quad c_{x1a} = -\infty, \\ &c_{x2a} = 0, \quad \phi_C\left(\theta, c_p, c_x\right) = c_x \\ &D: \theta_{1D} = 0, \quad \theta_{2D} = \pi/2, \quad c_{x1a} = -\infty, \\ &c_{x2a} = \infty, \quad \phi_D\left(\theta, c_p, c_x\right) = c_p \cos\theta \\ &E: \theta_{1E} = 0, \quad \theta_{2E} = \pi, \quad c_{x1a} = 0, \\ &c_{x2a} = \infty, \quad \phi_E\left(\theta, c_p, c_x\right) = c_x. \end{aligned} \tag{24}$$

All of the above integrals are calculated numerically for consistency reasons.

Finally, at the axis of symmetry ($r = 0$), denoted in Fig. 1 as (H), molecules are reflected specularly, i.e.

$$h^+_H\left(c_p, \theta, c_x\right) = h^-_H\left(c_p, \pi - \theta, c_x\right) \tag{25}$$

where $\theta \in [0, \pi/2]$.

3. Numerical scheme

3.1. Iterative algorithm and discretisation

The numerical scheme is based on the Discrete Velocity Method for the treatment of the three-dimensional molecular velocity space. The continuum spectrum of the cylindrical components c_p and c_x is discretised by the Legendre polynomial roots mapped in $\left[0, c_{p,\max}\right]$ and $\left[0, c_{x,\max}\right]$ respectively, while the molecular velocity angles are uniformly distributed in $[0, \pi]$ due to the axisymmetrical properties of the flow. The solution is obtained by an iterative procedure, where the main unknown is the distribution function. Initially, the perturbation of density is set equal to unity upstream, zero downstream and varies linearly along the tube, while the perturbations of velocity and temperature are zero everywhere. This estimation is chosen in order to accelerate convergence and is used in combination with the governing equation (6) to calculate the value of the distribution function h. The distribution function is further used to generate new values for the bulk quantities via the corresponding moments (7)–(10). These quantities are re-used in the governing equation to obtain new estimates for h and this procedure is repeated until a proper convergence criterion, imposed on the bulk quantities, is satisfied. A second order discretisation scheme has been applied in the two-dimensional physical space, derived in the same way as in [59] by integrating the governing equation in r, θ, x in an arbitrary discretisation interval, acting in both parts of (6) with the operator

$$A = \int_{x_k - \Delta x_k/2}^{x_k + \Delta x_k/2} \int_{\theta_j - \Delta\theta_j/2}^{\theta_j + \Delta\theta_j/2} \int_{r_i - \Delta r_i/2}^{r_i + \Delta r_i/2} (\cdot)\, dr d\theta dx. \tag{26}$$

Then, all integrations can either be carried out analytically, by eliminating the derivatives, or numerically by the trapezoidal rule, using the values of the distribution at the limits of the discretisation interval, e.g. at $x_k - \Delta x_k/2$, $x_k + \Delta x_k/2$. The trapezoidal rule is thus causing the second-order error. The final discretised expression is

$$\begin{aligned} &\frac{c_p^l \cos\theta_j}{4\Delta r_i}\left(h^{l,m}_{i+,j+,k+} + h^{l,m}_{i+,j-,k+} - h^{l,m}_{i-,j+,k+} - h^{l,m}_{i-,j-,k+}\right. \\ &\quad + h^{l,m}_{i+,j+,k-} + h^{l,m}_{i+,j-,k-} - h^{l,m}_{i-,j+,k-} - h^{l,m}_{i-,j-,k-}\Big) \\ &\quad - \frac{c_p^l \sin\theta_j}{4\Delta\theta_j}\left[\frac{1}{r_{i+}}\left(h^{l,m}_{i+,j+,k+} - h^{l,m}_{i+,j-,k+} + h^{l,m}_{i+,j+,k-}\right.\right. \\ &\quad \left. - h^{l,m}_{i+,j-,k-}\right) + \frac{1}{r_{i-}}\left(h^{l,m}_{i-,j+,k+} - h^{l,m}_{i-,j-,k+}\right. \\ &\quad \left.\left. + h^{l,m}_{i-,j+,k-} - h^{l,m}_{i-,j-,k-}\right)\right] \\ &\quad + \frac{c_x^m}{4\Delta x_k}\left(h^{l,m}_{i+,j+,k+} + h^{l,m}_{i+,j-,k+} + h^{l,m}_{i-,j+,k+} + h^{l,m}_{i-,j-,k+}\right. \\ &\quad \left. - h^{l,m}_{i+,j+,k-} - h^{l,m}_{i+,j-,k-} - h^{l,m}_{i-,j+,k-} - h^{l,m}_{i-,j-,k-}\right) \\ &\quad + \frac{\delta}{8}\left(h^{l,m}_{i+,j+,k+} + h^{l,m}_{i+,j-,k+} + h^{l,m}_{i-,j+,k+} + h^{l,m}_{i-,j-,k+}\right. \\ &\quad \left. + h^{l,m}_{i+,j+,k-} + h^{l,m}_{i+,j-,k-} + h^{l,m}_{i-,j+,k-} + h^{l,m}_{i-,j-,k-}\right) \\ &= \frac{\delta}{8}\left\{\left(\rho_{i+,k+} + \rho_{i-,k+} + \rho_{i+,k-} + \rho_{i-,k-}\right)\right. \\ &\quad + \left[\left(c_p^l\right)^2 + \left(c_x^m\right)^2 - \frac{3}{2}\right] \\ &\quad \times \left(\tau_{i+,k+} + \tau_{i-,k+} + \tau_{i+,k-} + \tau_{i-,k-}\right) \\ &\quad + 2c_p^l \cos\theta_j \left(u_{r,i+,k+} + u_{r,i-,k+} + u_{r,i+,k-} + u_{r,i-,k-}\right) \\ &\quad \left. + 2c_x^m \left(u_{x,i+,k+} + u_{x,i-,k+} + u_{x,i+,k-} + u_{x,i-,k-}\right)\right\}. \end{aligned} \tag{27}$$

In this discretised form, the indices i, k refer to the physical grid, l, m refer to the discrete velocity magnitudes c_p and c_x respectively, while j refers to the discrete velocity angle. The sign

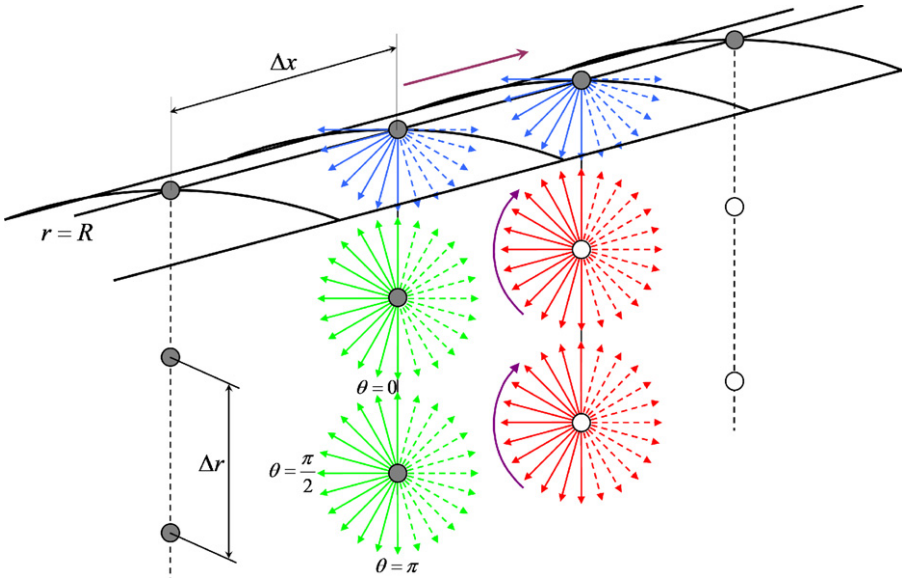

Fig. 2. Schematical representation of the marching scheme. (For interpretation of the references to colour in this figure legend, the reader is referred to the web version of this article.)

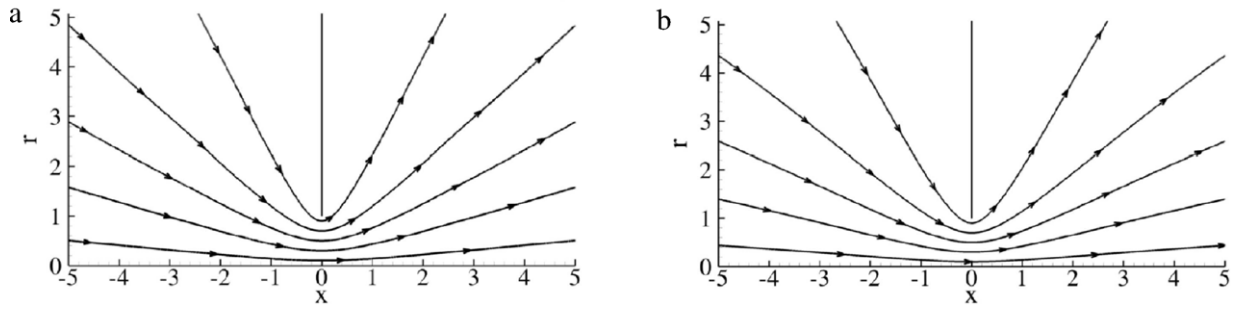

Fig. 3. Streamlines for $L/R = 0$ with (a) $\delta = 0.1$ and (b) $\delta = 10$.

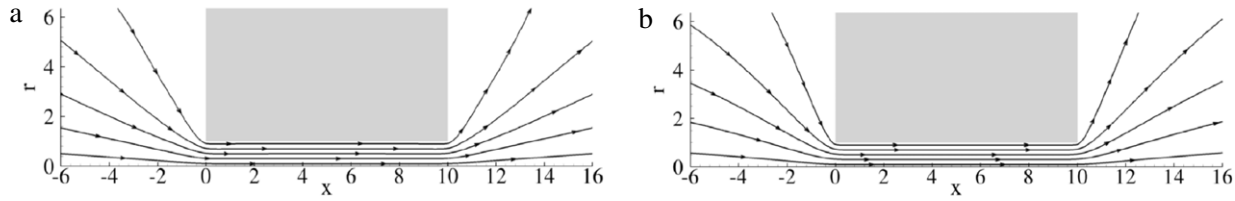

Fig. 4. Streamlines for $L/R = 10$ with (a) $\delta = 0.1$ and (b) $\delta = 10$.

following some indices indicates the position of the grid point in comparison to the discretisation point, for example $h^{l,m}_{i+,j+,k+} = h\left(r_i + \frac{\Delta r_i}{2}, x_k + \frac{\Delta x_k}{2}, c^l_p, \theta_j + \frac{\Delta \theta_j}{2}, c^m_x\right)$. It is also noted that the values of the distribution function are stored only on the limits of the discretisation interval, $(i\pm, j\pm, k\pm)$ and not on the central point (i, j, k). This expression is applied for any interval, regardless of the grid distances Δr_i, Δx_k and the angle discretisation $\Delta\theta_j$. It is also usable for intervals containing grid points with $r = 0$ after the application of the l'Hospital rule on the indeterminate fractions.

3.2. Parallelisation and memory handling

The computational effort can be distributed in several processors by noticing that the distribution functions of different velocity magnitudes can be calculated independently from one another [60]. As a result, the code can be easily parallelised in the molecular velocity space. Each processor solves the kinetic equation for a group of velocities and information on macroscopic quantities and impermeability constants is exchanged between the processors at the end of each iteration. In this manner, the transmission of the distribution is circumvented, greatly reducing the cost of parallel communication. The parallelisation algorithm has been tested in other problems [41] with several processors, displaying very good scaling characteristics (e.g. 94% efficiency for 64 cores). For parallelisation of even larger scale, the parallelisation may be extended in the physical space.

Memory handling techniques have also been used to reduce storage requirements because of the five-dimensional nature of the distribution function for this problem. Due to the velocity magnitude independency, a temporary array can be allocated and overwritten after treating each magnitude. Furthermore, the dimensionality of this array can be reduced even more by storing the distribution only in the parts of the domain required by the marching scheme of the discretised governing equation. For example, as seen in Fig. 2, the distribution is stored only at positions x

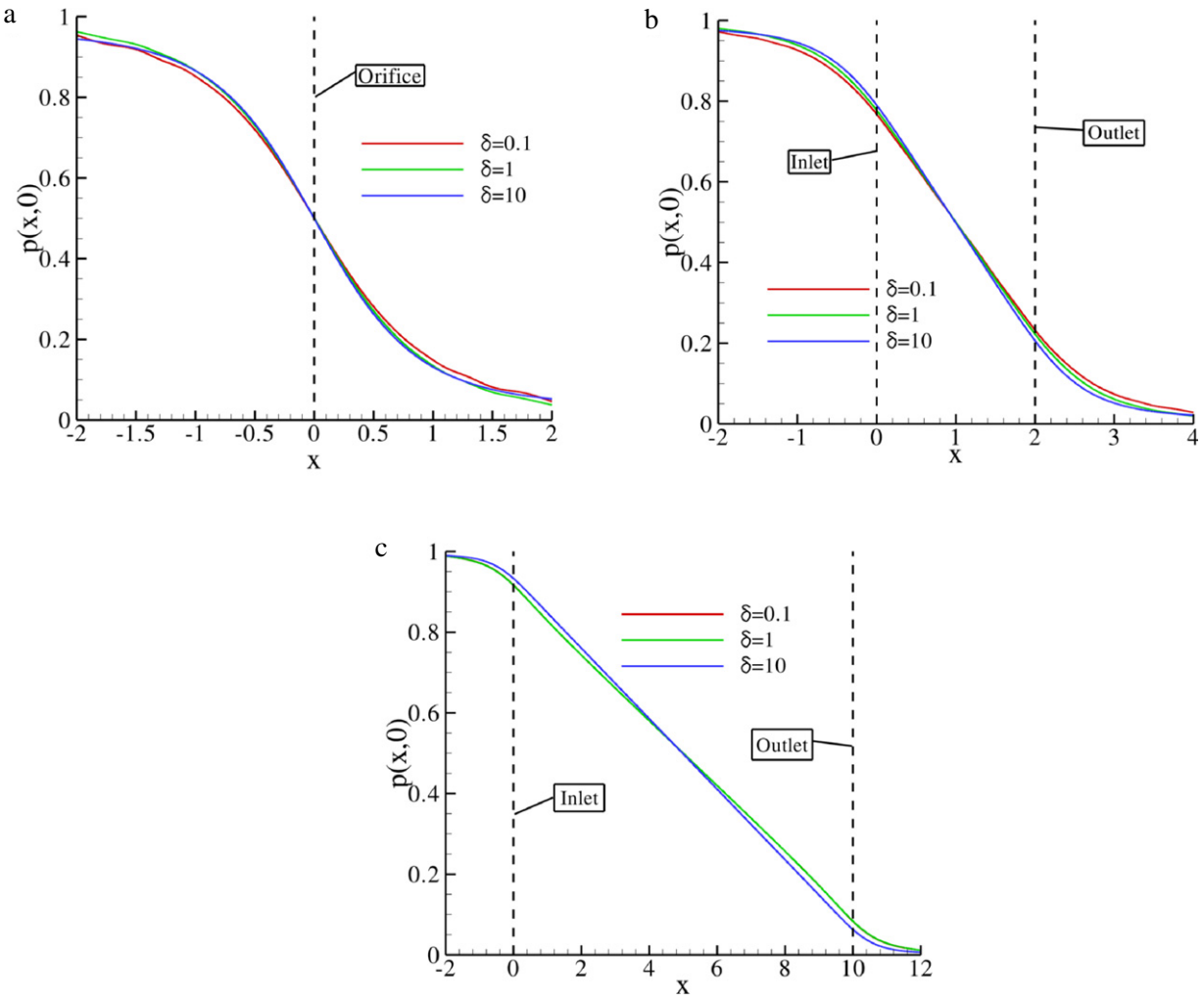

Fig. 5. Pressure perturbation distributions at the symmetry axis with (a) $L/R = 0$, (b) $L/R = 2$ and (c) $L/R = 10$ (the results for $\delta = 0.1$ and $\delta = 1$ coincide).

(red arrows) and $x - \Delta x$ (green arrows), for motion towards the positive x direction. Blue arrows indicate the boundary conditions, while dashed arrows denote the symmetrical parts of the distribution which are also neglected. These techniques permit having a two-dimensional array for the distribution function and greatly reduce memory limitations. In this manner, tubes of large L/R ratios can be considered, since the size of the distribution array is only determined by the height of the entrance/exit regions and the number of the molecular velocity angles.

3.3. Computational grid, numerical parameters and benchmarking

The computational grid was non-uniform, with particular emphasis on the accuracy near the wall corners. The discretisation intervals vary according to

$$\Delta x_i = \Delta x_0 \, (1 + \eta)^i \tag{28}$$

and similarly for the r-direction. The smallest intervals Δx_0, Δr_0 are close to the corners. It is well known [47] that the upstream/downstream regions must be quite large, since the mass conservation law indicates that the macroscopic quantities converge to the uniform container values at a very high distance from the tube. Therefore, container regions of size $L_{con} = R_{con} = 50R$ were used, after verifying that results do not change for larger values by parameterisation runs.

The average residual per node has been chosen as a convergence criterion

$$\text{residual} = \frac{1}{4N_{total}} \sum_{i=1}^{N_{total}} \left[\left| \rho_i - \rho_i^{pr} \right| + \left| \tau_i - \tau_i^{pr} \right| + \left| u_{r,i} - u_{r,i}^{pr} \right| + \left| u_{x,i} - u_{x,i}^{pr} \right| \right] \tag{29}$$

where the pr superscript denotes the corresponding quantities in the previous iteration and N_{total} is the total number of nodes. The discretisation parameters used are displayed in Table 1. For the results shown here, 150–200 intervals have been used in the first unit length around the corners, with the number of total physical nodes varying between 6×10^5 and 10^6. The number of discrete velocities ranged between 38,400 and 51,200. A typical computational iteration takes approximately 140–150 s with 32 CPU cores. The total number of iterations needed to reach convergence depends strongly on δ. Indicatively, for the satisfaction of the criterion shown in Table 1, it is around 100, 3000 and 10,000 for $\delta = 0.1$, 1 and 10, respectively. The dependence on the tube length is weaker, due to the fact that the initial condition of linear distribution within the channel approximates better the final solution for longer tubes.

The fulfilment of the mass conservation principle

$$\frac{1}{r} \frac{\partial \left(r u_r \right)}{\partial r} + \frac{\partial u_x}{\partial x} = 0 \tag{30}$$

which has been obtained by taking the appropriate moment of Eq. (6) in the molecular velocity space, was examined by calculating the left hand side of Eq. (30) in the whole field. It was shown

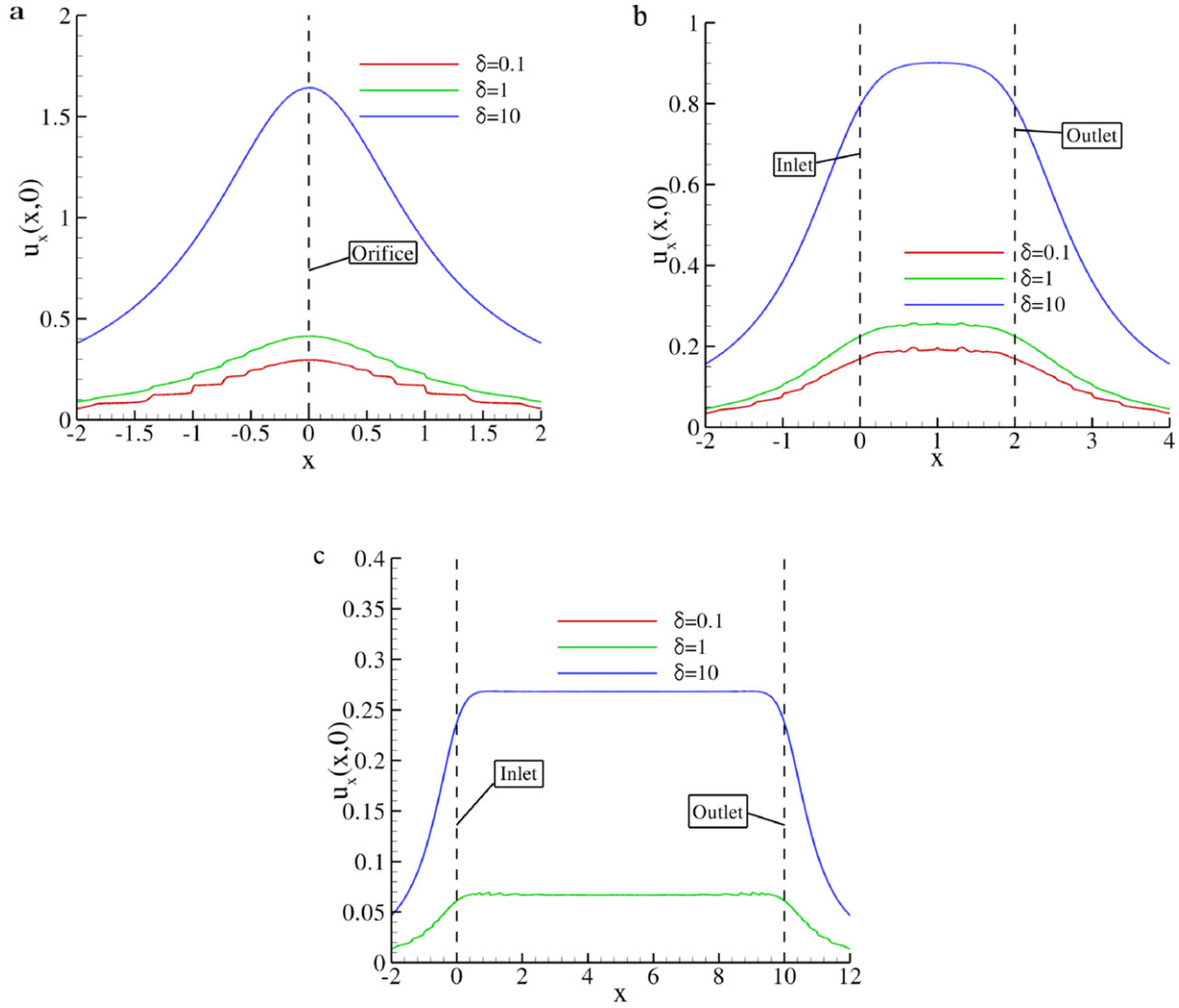

Fig. 6. Axial velocity distributions at the symmetry axis with (a) $L/R = 0$, (b) $L/R = 2$ and (c) $L/R = 10$ (the results for $\delta = 0.1$ and $\delta = 1$ coincide).

Table 1
Computational parameters.

Minimum physical space interval $\Delta x_0 = \Delta r_0$	6.7×10^{-3}
Physical discretisation increment factor η	10^{-2}
Discrete velocity angles N_θ in $(0, \pi)$	150–200
Discrete velocity components c_p and c_x	16×16
Maximum value of velocity components $c_{p,\max}$ and $c_{x,\max}$	5
Convergence criterion (residual)	10^{-8}–10^{-9}

that all values are very close to zero. Furthermore, the flow rate G given by Eq. (14) was calculated for all cases in several positions along the tube and it was found to be constant in at least three significant figures. Finally, the free molecular solution is retrieved with very good accuracy.

Overall the numerical results presented in the next section are considered accurate up to 3 significant figures within (± 1) in the last figure.

4. Results and discussion

4.1. Flow rates

Results for the dimensionless flow rate W_{LIN} are presented in Table 2 for various values of the reference rarefaction parameter δ and the length of the tube L/R, representing flows from the free molecular up to the slip regime through orifices and tubes

Table 2
Dimensionless flow rate W_{LIN} for various values of δ and L/R, with purely diffuse reflection ($\alpha_M = 1$).

δ	L/R						
	0	0.5	1	2	5	10	20
0	0.999	0.801	0.672	0.514	0.311	0.191	0.110
0.01	1.00	0.805	0.675	0.516	0.311	0.191	0.109
0.1	1.04	0.833	0.696	0.530	0.316	0.192	0.108
0.5	1.19	0.947	0.786	0.589	0.341	0.201	0.111
1	1.37	1.08	0.892	0.660	0.373	0.217	0.118
2	1.72	1.35	1.10	0.799	0.440	0.251	0.136
5	2.77	2.13	1.70	1.20	0.642	0.362	0.195
10	4.35	3.32	2.63	1.86	0.988	0.554	0.296

of small and moderate length. In particular, $\delta = [0, 0.01, 0.1, 0.5, 1, 2, 5, 10]$ and $L/R = [0, 0.5, 1, 2, 5, 10, 20]$, while purely diffuse reflection is assumed on the wall and $\alpha_M = 1$. It is seen that, at each value of δ, the flow rate W_{LIN} is decreased as L/R is increased. This is well expected since as the channel length is increased the local pressure gradient is reduced while the wall friction is increased, leading to lower bulk velocities. However, W_{LIN} is not directly proportional to the inverse of L/R. With regard to δ, it is seen that for each $0 \le L/R \le 10$ the flow rate W_{LIN} is monotonically increased along with the rarefaction parameter δ, while for $L/R = 20$ the Knudsen minimum phenomenon, well known in the case of long tubes, is observed. Thus, for $L/R = 20$ and starting from the free molecular limit ($\delta = 0$), the flow rate is slightly decreased

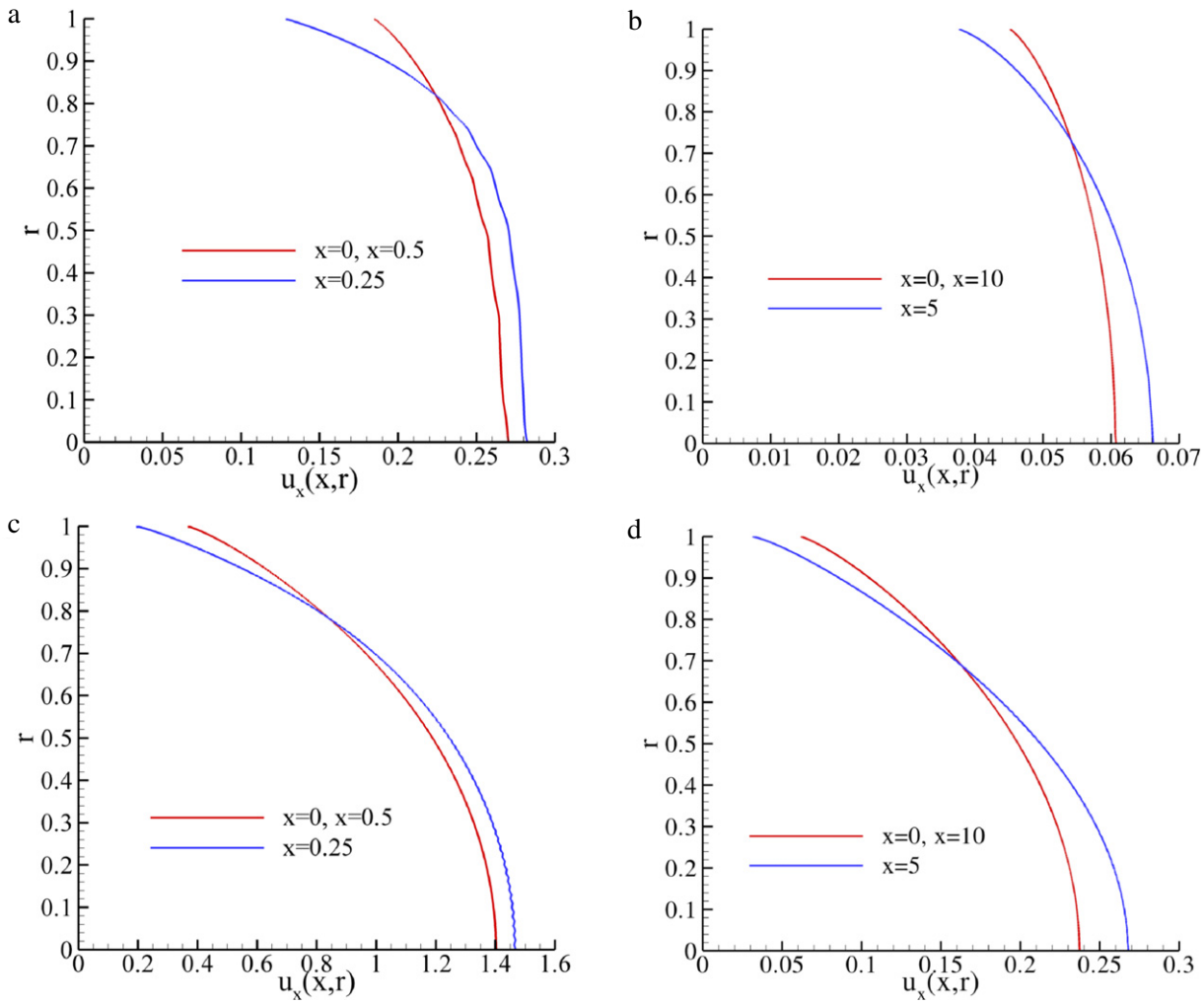

Fig. 7. Axial velocity distributions at various positions for $\delta = 0.1$ with (a) $L/R = 0.5$ and (b) $L/R = 10$ and for $\delta = 10$ with (c) $L/R = 0.5$ and (d) $L/R = 10$.

up to $\delta = 0.1$ and then it is increased along with δ. It is noted that the Knudsen minimum is very shallow compared to the one observed in tubes of infinite length and it appears to a smaller value of the rarefaction parameter (somewhere in the range $\delta = 0.1$–0.5) than expected.

Indicative results for incomplete accommodation are presented in Table 3, where the dimensionless flow rate W_{LIN} is tabulated for $\delta = [0, 0.1, 1, 10]$ and $L/R = [0, 1, 10]$, with $\alpha_M = [0.5, 0.8]$. It is seen that in the case of $L/R = 0$ the flow rate remains constant for all values of the accommodation coefficient (see also the fully accommodated results of Table 2) and therefore is practically independent of the wall accommodation properties. This is one of the favourable properties of orifice flow, making it an ideal configuration for the evaluation of numerical schemes, kinetic models and intermolecular potentials, as well as for comparison with experimental data, since the factor of gas-surface interaction can be neglected in this case. Similar properties have been found for slit flow [48]. For a tube of finite length, W_{LIN} is increased as α_M is decreased and the interaction becomes more specular. This trend is more dominant as δ is decreased and L/R is increased, which is expected since surface accommodation properties play a more important role for highly rarefied atmospheres and longer channels.

In order to estimate the introduced error when the assumption of fully developed flow (i.e. $L/R \to \infty$) is applied to channels of moderate length, a comparison with corresponding results of the present work is performed. In Table 4 the flow rate W_{FD}, obtained by the linearised formulation for fully developed flow is shown for the two longest tubes examined here ($L/R = 10, 20$) and for the same range of the rarefaction parameter ($0 \le \delta \le 10$). The quantities in parenthesis refer to the relative deviation, which has been obtained by comparing the fully developed results of Table 4 with the corresponding ones in Table 2.

Table 3
Dimensionless flow rate W_{LIN} for various values of δ and L/R, with diffuse-specular reflection ($\alpha_M \neq 1$).

		L/R					
		0		1		10	
α_M		0.5	0.8	0.5	0.8	0.5	0.8
δ	0	1.00	0.999	0.814	0.726	0.368	0.247
	0.1	1.04	1.04	0.840	0.751	0.368	0.247
	1	1.37	1.37	1.07	0.955	0.402	0.271
	10	4.35	4.35	3.03	2.76	0.786	0.617

It is seen that the agreement is improved as L/R and δ are increased. This is reasonable since, as the length of the tube is increased, the channel ends affect a relatively smaller part of the geometry, while high values of δ result in smaller flow development lengths and therefore faster adaptation to the fully developed flow profile. The maximum deviation, which is 39.8%, occurs for $L/R = 10$ and $\delta = 0$ as it could be expected, while the minimum one is 6.7% and is found for $L/R = 20$ and $\delta = 10$. These results provide an estimate of the accuracy to expect when fully developed solutions are implemented in rarefied flows

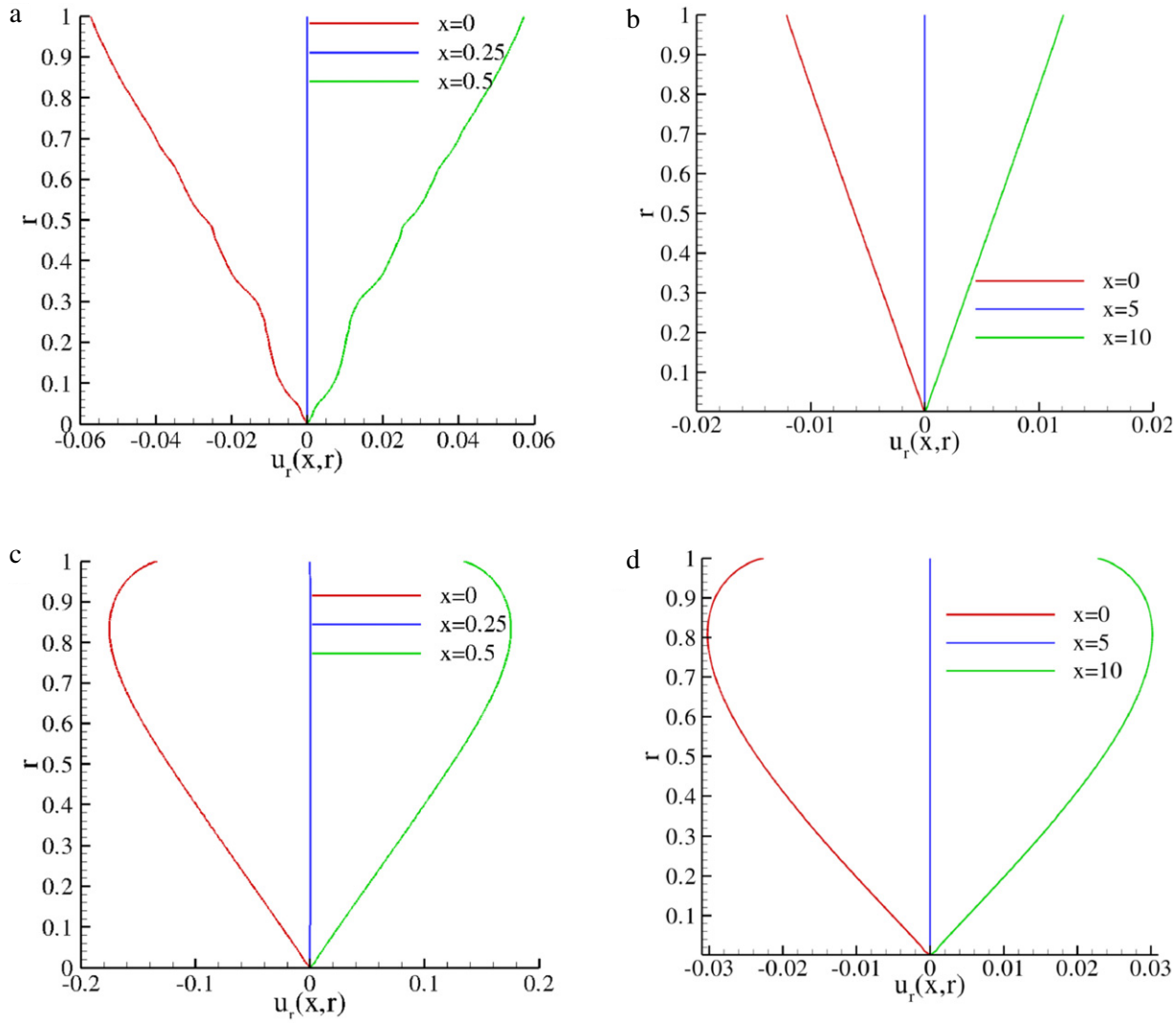

Fig. 8. Radial velocity distributions at various positions for $\delta = 0.1$ with (a) $L/R = 0.5$ and (b) $L/R = 10$ and for $\delta = 10$ with (c) $L/R = 0.5$ and (d) $L/R = 10$.

Table 4
Dimensionless flow rate W_{FD} for various values of δ and L/R, obtained by the fully developed flow approximation, with purely diffuse reflection ($\alpha_M = 1$); the numbers in parenthesis denote the corresponding relative error.

δ	L/R	
	10	20
0	0.267 (39.8%)	0.133 (20.9%)
0.01	0.262 (37.2%)	0.131 (20.2%)
0.1	0.249 (29.7%)	0.124 (14.8%)
0.5	0.246 (22.4%)	0.123 (10.8%)
1	0.258 (18.9%)	0.129 (9.3%)
2	0.294 (17.1%)	0.147 (8.1%)
5	0.416 (14.9%)	0.208 (6.7%)
10	0.632 (14.1%)	0.316 (6.7%)

through circular channels of moderate length due to small pressure differences.

4.2. Macroscopic distributions

Streamline plots are shown in Figs. 3 and 4 for $L/R = 0$, 10 and $\delta = 0.1$, 10. These streamlines are indicative for the other values of L/R and δ used in this work. It is confirmed that the impermeability condition is always satisfied, producing completely horizontal lines inside the channel, even for the demanding case of the relatively long channels. The streamlines are symmetrical around $x = L/(2R)$ and structures appearing in non-linear flows, such as vortices, are absent.

The distributions of perturbed pressure and axial velocity along $r = 0$ are shown in Figs. 5 and 6 respectively for several values of L/R and δ. The perturbed pressure far upstream is equal to unity, then it is reduced through the tube and finally becomes zero far downstream. It is seen that the pressure profiles for each L/R are quite similar for all values of δ. Also, they vary nearly linear at the centre of the channel. This is more evident in the case of the long tube $L/R = 10$ and it is reasonable since in this case the hypothesis of fully developed flow is practically fulfilled. The differences are mostly located in the gradient of pressure, determining the flow rate. The axial velocity far upstream is zero, then it is increased up to $x = L/(2R)$ where its maximum value is reached and finally it is decreased to zero far downstream. For $L/R = 10$ the axial velocity reaches a plateau after a distance of around one tube radius from the inlet and then maintains this value for the rest of the tube, showing close resemblance to a fully developed profile. The perturbed pressure and reduced axial velocity are antisymmetric and symmetric respectively about $x = L/(2R)$.

The axial and radial macroscopic velocity component distributions are shown in Figs. 7 and 8 respectively at the entrance ($x = 0$), middle ($x = L/(2R)$) and exit ($x = L/R$) of the tubes with $L/R = 0.5$, 10 and $\delta = 0.1$, 10. Due to the properties of the

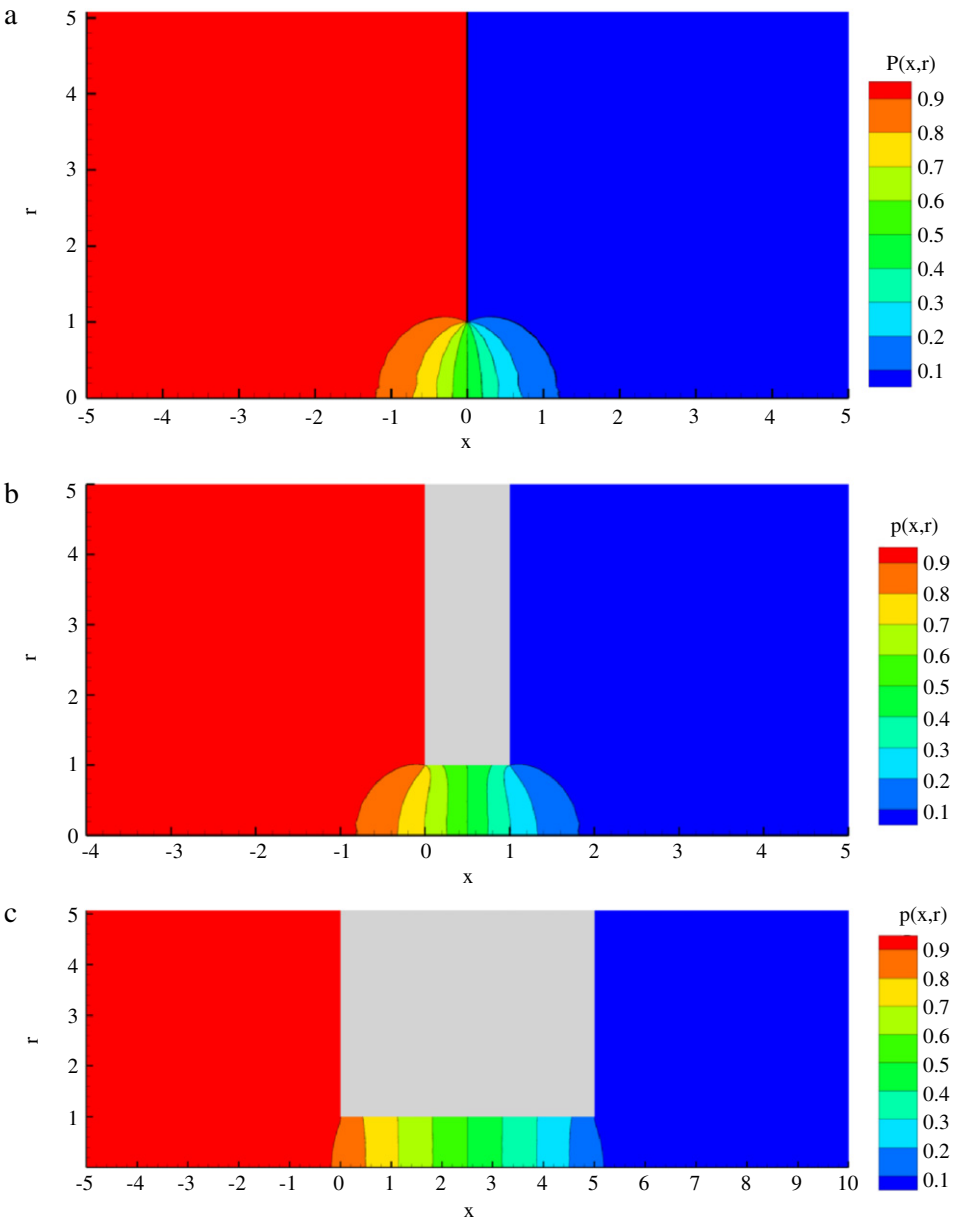

Fig. 9. Pressure perturbation for $\delta = 1$ with (a) $L/R = 0$, (b) $L/R = 1$, (c) $L/R = 5$.

flow, the axial velocity profile is identical at the entrance and exit of the tube (see Fig. 7), while the radial component is antisymmetric around the tube middle (see Fig. 8). For $\delta = 0.1$, the axial velocity takes small values distributed in a rather narrow range and characterised by a significant jump on the walls, while for $\delta = 10$ a more pronounced parabolic profile is obtained. The radial velocity distribution approaches a linear form for the most linear case ($\delta = 0.1$, $L/R = 10$), while it is always zero in the middle. In all cases, larger δ and smaller L/R lead to larger velocity magnitudes.

A more complete view of the flow field is presented in Figs. 9–12 for various values of δ and L/R. The effect of changing the tube length is examined for a constant rarefaction parameter $\delta = 1$, with $L/R = 0$, $L/R = 1$ and $L/R = 5$ in Figs. 9 and 10, where the corresponding pressure and axial velocity fields are shown. The pressure distribution around the channel ends gradually becomes closer to the container values as the length increases, i.e. the pressure contour colouring at each container is more uniform for $L/R = 5$ than for $L/R = 0, 1$. This happens because the area of the reservoirs affected by the channel flow is smaller for longer channels, due to the smaller induced gas velocities. Also, a small region of slightly higher and lower pressure than the container values is also observed just above the channel openings. The axial velocity is significantly reduced for longer tubes and seems to develop a nearly constant profile inside the channel and in a relatively short distance from the channel ends. The end influence on the velocity profile seems to fade away around one unit of dimensionless length inside the channel for $L/R = 5$ and $\delta = 1$. The effect of changing the rarefaction parameter δ is shown in Figs. 11 and 12 for a tube of $L/R = 2$, with $\delta = 0.1$, 1 and 10. No significant changes occur for the pressure perturbations, besides a slightly larger deviation of pressure in the containers from the equilibrium values as δ is increased. The axial velocity values are increased along with δ.

It is noted that the non-smooth distributions of the macroscopic quantities in Figs. 5–12 are caused by the so-called ray effects. These are present mainly at $\delta = 0.1$, caused by the boundary induced discontinuities of the distribution function which propagate through the flow field and become more dominant at small values

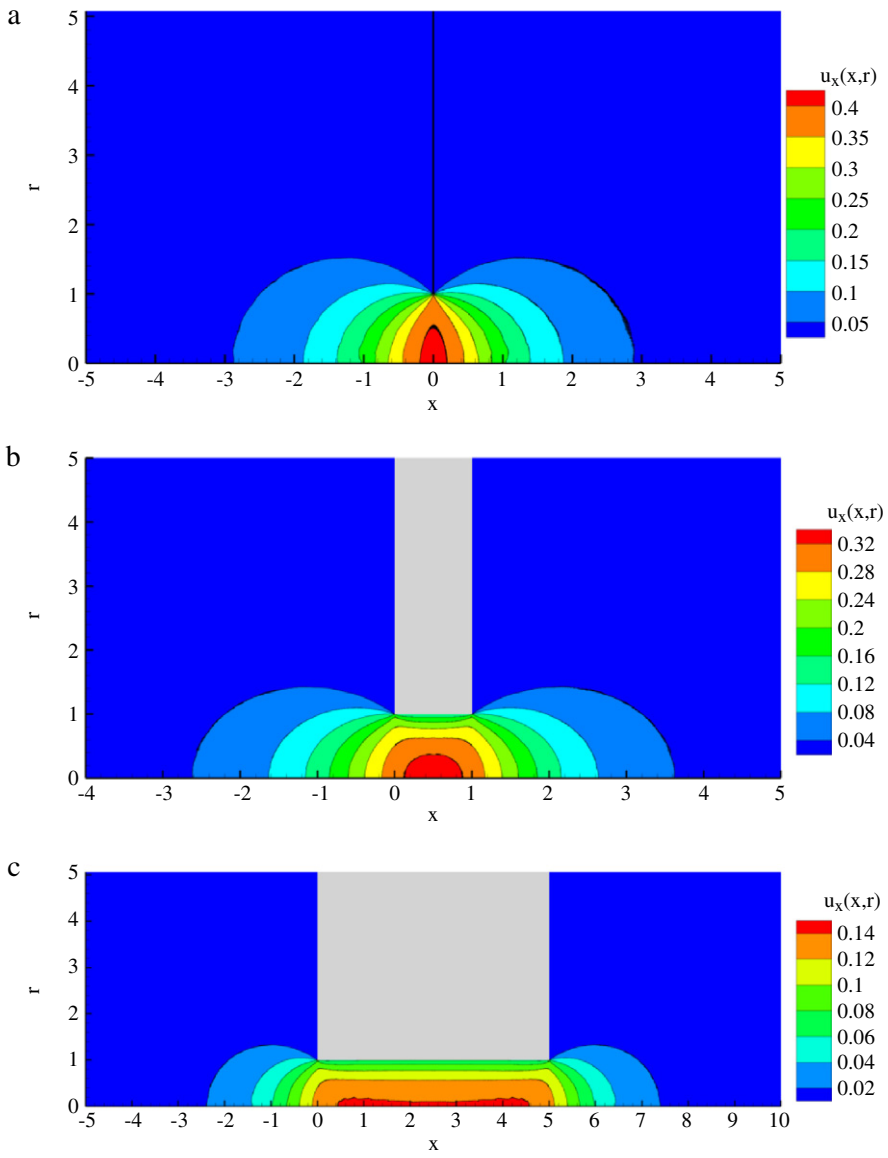

Fig. 10. Axial velocity for $\delta = 1$ with (a) $L/R = 0$, (b) $L/R = 1$, (c) $L/R = 5$.

of δ. This is a disadvantage of the discrete velocity method, which is not easily circumvented. However, it is expected to have no significant effect on overall quantities, such as the flow rate.

4.3. Comparison with non-linear results

In this subsection, a comparison of the present linear flow rates with corresponding ones based on the non-linear BGK equation, denoted by W_{NL}, is presented. For this purpose the flow rates W_{NL} for $P_2/P_1 = 0.9$ (or $\Delta P/P_0 = 0.1$) and $L/R = 0, 1, 5$ are tabulated in Table 5. The results have been obtained by the non-linear BGK model [61] and have been found to be in very good agreement with corresponding DSMC results [35].

It is seen that the agreement between the linear flow rates W_{LIN} and the corresponding non-linear ones W_{NL} is very good in general. The differences between are reduced as δ is decreased and as L/R is increased. This trend is explained since as the gas becomes more rarefied and the tube longer the bulk velocity is decreased leading to small Mach and Reynolds numbers and to a linear symmetric flow field. In several cases the agreement is good to all three significant figures shown, while the worst case is for $\delta = 10$ and $L/R = 0$, where the relative error is about 2.5%. Obviously, as the pressure difference is decreased the agreement will be also significantly improved.

Table 5
Dimensionless flow rate W_{NL} for various values of δ and L/R with $P_2/P_1 = 0.9$ and $\alpha_M = 1$, obtained by the non-linear BGK model [61].

δ	L/R					
	0		1		5	
	W_{LIN}	W_{NL}	W_{LIN}	W_{NL}	W_{LIN}	W_{NL}
0	0.999	1.00	0.672	0.672	0.311	0.310
0.1	1.04	1.04	0.696	0.695	0.316	0.315
1	1.37	1.35	0.892	0.881	0.373	0.375
5	2.77	2.73	1.70	1.69	0.642	0.641
10	4.35	4.24	2.63	2.60	0.988	0.973

Based on the above it may be stated that for pressure ratio values up to $\Delta P/P_0 = 0.1$ the present BGK linear formulation gives satisfactory results in good agreement with the non-linear BGK formulations in the free molecular and transition regimes. This remark has two implications: First, linearised equations provide correct results at a wider range than expected from the

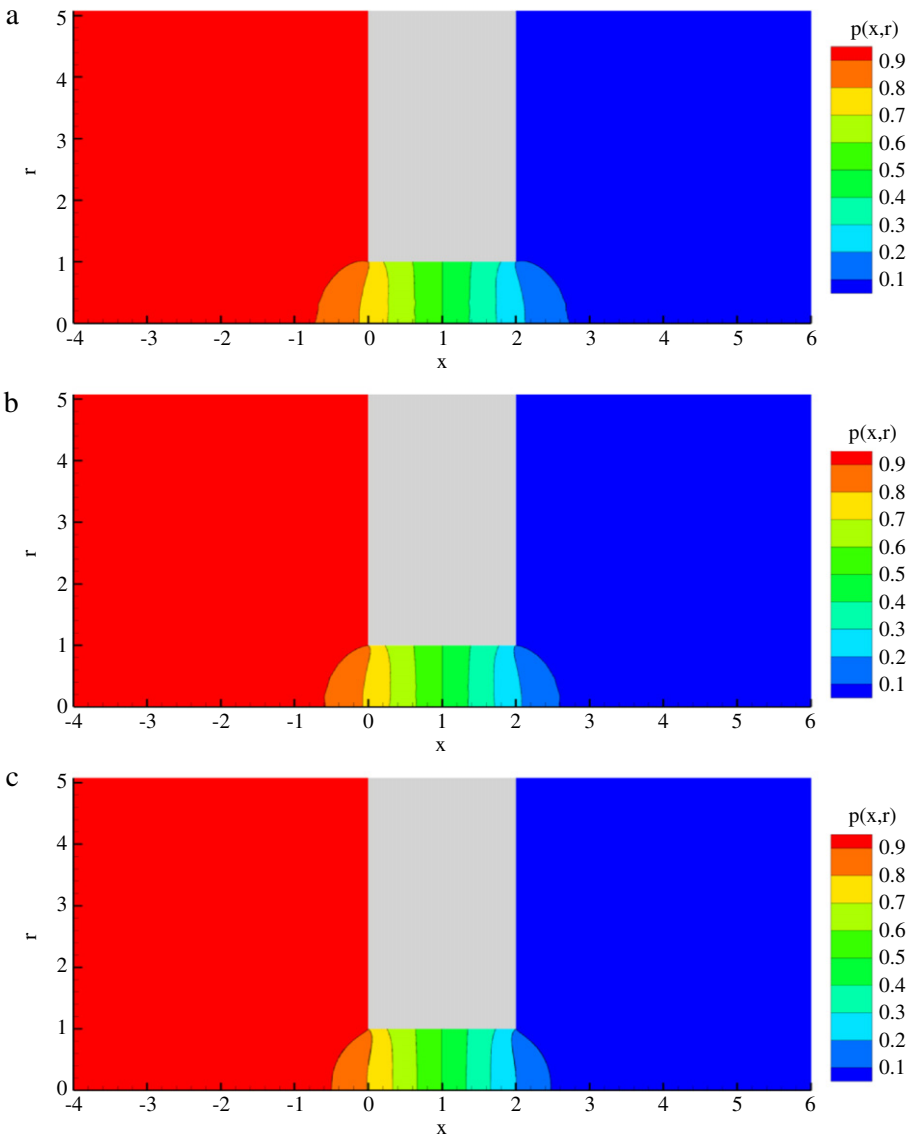

Fig. 11. Pressure perturbation with $L/R = 2$ and (a) $\delta = 0.1$, (b) $\delta = 1$, (c) $\delta = 10$.

mathematical derivation, i.e., the pressure difference must be small but finite and not infinitesimally small as specified by theory. Secondly, linearised theory can be used as a complimentary approach for a considerable range of pressure ratios, for which other computational methods, such as the DSMC method, become computationally inefficient. It is noted that the computational efficiency of the present DVM algorithm is practically independent of the pressure difference.

5. Concluding remarks

Rarefied gas flow through cylindrical tubes due to a small pressure difference has been investigated by the linearised BGK model subject to Maxwell diffuse-specular boundary conditions. The kinetic equations are solved by implementing an efficiently parallelised and memory storage handling discrete velocity algorithm. The investigation covers flow in the free molecular up to the slip regime through tubes of very short (including orifices) up to moderate lengths ($L/R = 20$).

The quantitative behaviour of the flow rate and the macroscopic distributions of pressure (or density) and velocity is examined in detail in terms of the rarefaction parameter δ and the tube length ratio L/R. The flow rate is monotonically increased for L/R below 20, where the Knudsen minimum shows up in the range $\delta = 0.1$–0.5. In the case of orifice flow ($L/R = 0$), it is confirmed that the results are practically independent of the accommodation coefficient, making this flow configuration very advantageous for benchmarking and comparison with experimental data. Comparing the present linear results with corresponding non-linear ones, it is seen that linear analysis can capture the correct behaviour of the flow field in the free molecular and transition regimes not only for infinitesimally small but also for small but finite pressure differences and it is argued that its range of applicability is wider than expected. This is very important because linear analysis has a solid and well known theoretical background, which is very helpful in the robust and reliable numerical solution of the governing kinetic equations. Finally, the introduced error when the assumption of fully developed flow is applied to channels of moderate length is estimated by a comparison with corresponding results is performed.

It is hoped that the present work may be useful in engineering applications as well as in comparisons with experimental results which are very limited in rarefied flows in the transition regime due to small pressure differences.

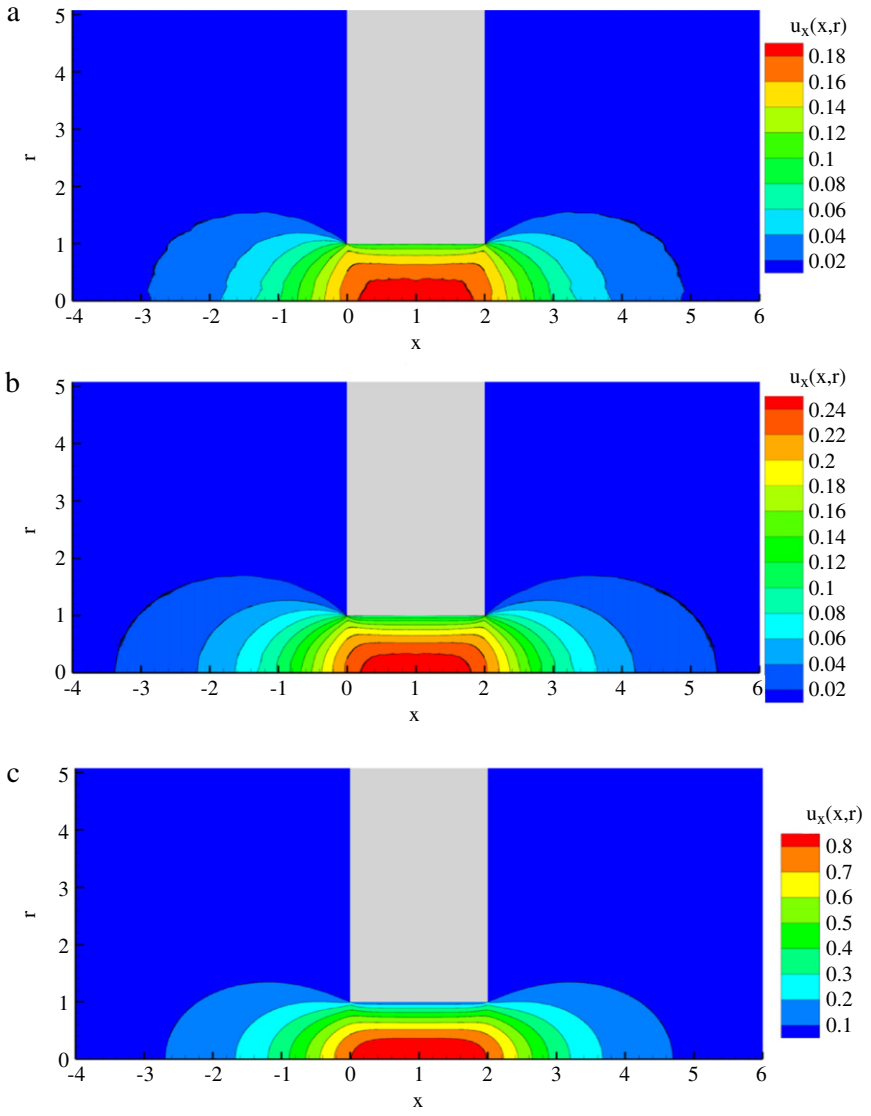

Fig. 12. Axial velocity with $L/R = 2$ and (a) $\delta = 0.1$, (b) $\delta = 1$, (c) $\delta = 10$.

Acknowledgments

The authors gratefully acknowledge support by the Association Euratom—Hellenic Republic. The views and opinions expressed herein do not necessarily reflect those of the European Commission.

References

[1] W. Jitschin, M. Ronzheimer, S. Khodabakhshi, Gas flow measurement by means of orifices and Venturi tubes, Vacuum 53 (1999) 181–185.
[2] X. Li, G.S. Oehrlein, M. Schaepkens, R.E. Ellefson, L.C. Frees, Spatially resolved mass spectrometric sampling of inductively coupled plasma using a movable sampling orifice, J. Vac. Sci. Technol., A 21 (2003) 1971–1977.
[3] A.A. Alexeenko, D.A. Levin, S.F. Gimelshein, M.S. Ivanov, A.D. Ketsdever, Numerical and experimental study of orifice flow in the transitional regime, in: AIAA Paper 2001, No. 3072, 2001.
[4] K. Aoki, P. Degond, S. Takata, H. Yoshida, Diffusion models for Knudsen compressors, Phys. Fluids 19 (2007) 117103.1–117103.21.
[5] K. Jousten, Handbook of Vacuum Technology, Wiley-VCH Verlag, Weinheim, 2008.
[6] S. Misdanitis, D. Valougeorgis, Design of steady-state isothermal gas distribution systems consisting of long tubes in the whole range of the Knudsen number, J. Vac. Sci. Technol., A 29 (6) (2011) 061602.1–061602.7.
[7] O. Aktas, N.R. Aluru, U. Ravaioli, Application of a parallel DSMC technique to predict flow characteristics in microfluidic filters, J. Microelectromech. Syst. 10 (4) (2001) 538–549.
[8] F. Hamad, K.C. Khulbe, T. Matsuura, Comparison of gas separation performance and morphology of homogeneous and composite PPO membranes, J. Membr. Sci. 256 (2005) 29.
[9] C.M. Ho, Y.C. Tai, Micro-electro-mechanical systems (MEMS) and fluid flows, Annu. Rev. Fluid Mech. 30 (1998) 579–612.
[10] S. Lorenzani, L. Gibelli, A. Frezzotti, A. Frangi, C. Cercignani, Kinetic approach to gas flows in microchannels, Nanoscale Microscale Thermophys. Eng. 11 (2007) 211–226.
[11] G.A. Bird, Transition regime behavior of supersonic beam skimmers, Phys. Fluids 19 (10) (1976) 1486–1491.
[12] K. Waichman, Kinetic study of the effects of boundary geometry on rarefied vapor flow, Phys. Fluids 8 (5) (1996) 1321–1329.
[13] G.D. Danilatos, M.R. Phillips, J.V. Nailon, Electron beam current loss at the high-vacuum-high-pressure boundary in the environmental scanning electron microscope, Microsc. Microanal. 7 (2001) 397–406.
[14] C. Cercignani, Rarefied gas flow through long slots, J. Appl. Math. Phys. (ZAMP) 30 (1979) 943–951.
[15] F. Sharipov, V. Seleznev, Rarefied gas flow through a long tube at any pressure ratio, J. Vac. Sci. Technol., A 12 (5) (1994) 2933–2935.
[16] K. Aoki, Dynamics of rarefied gas flows: asymptotic and numerical analyses of the Boltzmann equation, in: AIAA Paper 2001, No. 0874, 2001.
[17] S. Naris, D. Valougeorgis, F. Sharipov, D. Kalempa, Flow of gaseous mixtures through rectangular microchannels driven by pressure, temperature, and concentration gradients, Phys. Fluids 17 (10) (2005) 100607.1–100607.12.
[18] F. Sharipov, I. Graur, Gas flow through an elliptical tube over the whole range of the gas rarefaction, Eur. J. Mech. B/Fluids 27 (3) (2007) 335–345.
[19] S. Naris, D. Valougeorgis, Rarefied gas flow in a triangular duct based on a boundary fitted lattice, Eur. J. Mech. B/Fluids 27 (6) (2008) 810–822.
[20] G. Breyannis, S. Varoutis, D. Valougeorgis, Rarefied gas flow in concentric annular tube: estimation of the Poiseuille number and the exact hydraulic diameter, Eur. J. Mech. B/Fluids 27 (5) (2008) 609–622.

[21] S. Kosuge, S. Takata, Database for flows of binary gas mixtures through a plane microchannel, Eur. J. Mech. B/Fluids 27 (4) (2008) 444–465.
[22] S. Varoutis, S. Naris, V. Hauer, C. Day, D. Valougeorgis, Computational and experimental study of gas flows through long channels of various cross sections in the whole range of the Knudsen number, J. Vac. Sci. Technol., A 27 (1) (2009).
[23] F. Sharipov, V. Seleznev, Data on internal rarefied gas flows, J. Phys. Chem. Ref. Data 27 (3) (1998) 657–706.
[24] T. Ewart, P. Perrier, I.A. Graur, J.G. Meolans, Mass flow rate measurements in a microchannel, from hydrodynamic to near free molecular regimes, J. Fluid Mech. 584 (2007) 337–356.
[25] J. Pitakarnnop, S. Varoutis, D. Valougeorgis, S. Geoffroy, L. Baldas, S. Colin, A novel experimental setup for gas microflows, Microfluid. Nanofluid. 8 (2009) 57–72.
[26] S. Pantazis, S. Varoutis, V. Hauer, C. Day, D. Valougeorgis, Gas-surface scattering effect on vacuum gas flows through rectangular channels, Vacuum 85 (2011) 1161–1164.
[27] R. Narasimha, Orifice flow at high Knudsen numbers, J. Fluid Mech. 10 (1961) 371–384.
[28] D.R. Willis, Mass flow through a circular orifice and a two-dimensional slit at high Knudsen numbers, J. Fluid Mech. 21 (1) (1965) 21–31.
[29] J.D. Stewart, Mass flow rate for nearly-free molecular slit flow, J. Fluid Mech. 35 (3) (1969) 599–608.
[30] G.A. Bird, Molecular Gas Dynamics and the Direct Simulation of Gas Flows, Oxford University Press, Oxford, 1994.
[31] D.G. Wadsworth, D.A. Erwin, Numerical simulation of rarefied flow through a slit, part I: direct simulation Monte Carlo results, Phys. Fluids A 5 (1) (1993) 235–242.
[32] F. Sharipov, D.V. Kozak, Rarefied gas flow through a thin slit into vacuum simulated by the Monte Carlo method over the whole range of the Knudsen number, J. Vac. Sci. Technol., A 27 (3) (2009) 479–484.
[33] O. Sazhin, Gas molecule–molecule interaction and the gas-surface scattering effect on the rarefied gas flow through a slit into a vacuum, J. Exp. Theor. Phys. 108 (5) (2009) 874–879.
[34] H. Taniguchi, M. Ota, M. Aritomi, Effects of surface boundary conditions on transmition probabilities through circular tubes, Vacuum 47 (6–8) (1996) 787–790.
[35] F. Sharipov, Numerical simulation of rarefied gas flow through a thin orifice, J. Fluid Mech. 518 (2004) 35–60.
[36] T.C. Lilly, S.F. Gimelshein, A.D. Ketsdever, G.N. Markelov, Measurements and computations of mass flow and momentum flux through short tubes in rarefied gas, Phys. Fluids 18 (2006) 093601.1–093601.11.
[37] S. Varoutis, D. Valougeorgis, F. Sharipov, Simulation of gas flow through tubes of finite length over the whole range of rarefaction for various pressure drop ratios, J. Vac. Sci. Technol., A 27 (6) (2009) 1377–1391.
[38] E.M. Shakhov, Solution of axisymmetric problems of rarefied gas theory by a finite difference method, Comput. Math. Math. Phys. 14 (4) (1974) 970–981.
[39] P. Raghuraman, D.R. Willis, Kinetic theory analysis of rarefied gas flow through finite length slots, Phys. Fluids 20 (6) (1977) 895–902.
[40] V.A. Titarev, Conservative numerical methods for model kinetic equations, Comput. & Fluids 36 (9) (2007) 1446–1459.
[41] S. Pantazis, D. Valougeorgis, Efficient simulation of rarefied gas flows through tubes of finite length based on kinetic model equations, in: D.A. Levin, I.J. Wysong, A.L. Garcia, H. Abarbanel (Eds.) 27th International Symposium on Rarefied Gas Dynamics, AIP Conference Proceedings, 2010.
[42] I.A. Graur, A.P. Polikarpov, F. Sharipov, Numerical modelling of rarefied gas flow through a slit into vacuum based on the kinetic equation, Comput. & Fluids 49 (1) (2011) 87–92.
[43] S. Misdanitis, S. Pantazis, D. Valougeorgis, Pressure driven rarefied gas flow through a slit and an orifice, Vacuum 86 (11) (2012) 1701–1708.
[44] V.D. Akin'shin, V.D. Seleznev, F.M. Sharipov, Non-isothermal rarefied gas flow through a narrow slit, Translated from Mekhanika Zhidkosti i Gaza 4 (1991) 171–175.
[45] E.M. Shakhov, Approximate kinetic equations in rarefied gas theory, Fluid Dyn. 3 (1) (1968) 156–161.
[46] E.M. Shakhov, Generalization of the Krook kinetic equation, Fluid Dyn. 3 (5) (1968) 142–145.
[47] M. Hasegawa, Y. Sone, Rarefied gas flow through a slit, Phys. Fluids A 3 (3) (1990) 466–477.
[48] F. Sharipov, Rarefied gas flow through a slit, influence of the boundary conditions, Phys. Fluids 8 (1) (1996) 262–268.
[49] F. Sharipov, Non-isothermal rarefied gas flow through a slit, Phys. Fluids 9 (6) (1997) 1804–1810.
[50] E.M. Shakhov, Rarefied gas flow in a pipe of finite length, Comput. Math. Math. Phys. 40 (4) (2000) 618–626.
[51] E.M. Shakhov, Rarefied flow in a channel and a periodic system of channels, Fluid Dyn. 35 (3) (2000) 449–456.
[52] H.W. Liepmann, Gas kinetic and gas dynamics of orifice flow, J. Fluid Mech. 10 (1961) 65–79.
[53] A.K. Sreekanth, Transition flow through short circular tubes, Phys. Fluids 8 (11) (1965) 1951–1956.
[54] T. Fujimoto, M. Usami, Rarefied gas flow through a circular orifice and short tubes, ASME, Transactions, J. Fluids Eng. 106 (1984) 367–373.
[55] L. Marino, Experiments on rarefied gas flows through tubes, Microfluid. Nanofluid. 6 (2009) 109–119.
[56] S. Varoutis, V. Hauer, C. Day, S. Pantazis, D. Valougeorgis, Experimental and numerical investigation in flow configurations related to the vacuum systems of fusion reactors, Fusion Eng. Des. 85 (10–12) (2010) 1798–1802.
[57] S.F. Borisov, I.G. Neudachin, B.T. Porodnov, P.E. Suetin, Flow of rarefied gases through an orifice for small pressure drop, Tech. Phys. 43 (1973) 1735–1739. (in Russian).
[58] B.T. Porodnov, P.E. Suetin, S.F. Borisov, V.D. Akinshin, Experimental investigation of rarefied gas flow in different channels, J. Fluid Mech. 64 (1974) 417–437.
[59] S. Pantazis, D. Valougeorgis, Heat transfer through rarefied gases between coaxial cylindrical surfaces with arbitrary temperature difference, Eur. J. Mech. B/Fluids 29 (6) (2010) 494–509.
[60] V.V. Aristov, S.A. Zabelok, A deterministic method for solving the Boltzmann equation with parallel computations, Comput. Math. Math. Phys. 42 (3) (2002) 406–418.
[61] S. Pantazis, Simulation of transport phenomena in conditions far from thermodynamic equilibrium via kinetic theory with applications in vacuum technology and MEMS, Volos, Greece: Ph.D. Dissertation, University of Thessaly, 2011.